**DELPHI Collaboration** DELPHI 2002-028 CONF 562
4 July, 2002

# Measurement of the Forward-Backward Asymmetries of $e^+e^- \rightarrow Z \rightarrow b\bar{b}$ and $e^+e^- \rightarrow Z \rightarrow c\bar{c}$ using prompt leptons

**P. Antilogus** [1], **E. Migliore** [2], **M. Paganoni** [3]

[1] Université Claude Bernard de Lyon, IPNL, IN2P3-CNRS, F69622 Villeurbanne Cedex, France

[2] Dipartimento di Fisica Sperimentale, Università di Torino and INFN, I10125 Turin, Italy

[3] Dipartimento di Fisica, Università di Milano and INFN Sezione di Milano, I20133 Milan, Italy

**Abstract**

The forward-backward asymmetries of the processes $e^+e^- \rightarrow Z \rightarrow b\bar{b}$ and $e^+e^- \rightarrow Z \rightarrow c\bar{c}$ were measured from a sample of hadronic $Z$ decays collected by the DELPHI experiment between 1993 and 1995. Enriched samples of $b\bar{b}$ and $c\bar{c}$ events were obtained using lifetime information. The tagging of $b$ and $c$ quarks in these samples was based on the semileptonic decay channels $b/c \rightarrow X + \mu$ and $b/c \rightarrow X + e$ combined with charge flow information from the hemisphere opposite to the lepton.

Averaging the $A_{\rm FB}^{\rm b\bar{b}}$ and $A_{\rm FB}^{\rm c\bar{c}}$ measurements presented in this paper with results published based on 1991 and 1992 DELPHI data sample, the following pole asymmetries were obtained :

$$\begin{array}{lcrcrcrc} A_{\rm FB}^{0,b} & = & 0.1021 & \pm & 0.0052 & (\rm stat) & \pm & 0.0024 \quad (\rm syst) \\ A_{\rm FB}^{0,c} & = & 0.0728 & \pm & 0.0086 & (\rm stat) & \pm & 0.0063 \quad (\rm syst) \end{array}$$

The effective value of the Weinberg mixing angle derived from these measurements was

$$\sin^2\theta_{\rm W,eff}^{lept} = 0.23169 \pm 0.00010$$

Contributed Paper for ICHEP 2002 (Amsterdam)

# 1 Introduction

The polar angle, $\theta$, of the final state fermion relative to the incoming electron in the reaction $e^+e^- \rightarrow f\overline{f}$ , at $\sqrt{s} \simeq M_Z$, is distributed according to:

$$\frac{\mathrm{d}\sigma}{\mathrm{d}\cos\theta} \propto 1 + \cos^2\theta + \frac{8}{3} A_{\mathrm{FB}}^{\mathrm{f\bar{f}}} \cos\theta \tag{1}$$

The coefficient of the parity violating term, in the Electroweak Standard Model and for pure $Z$ exchange, is related, at the lowest order, to the vector ($v_f$) and axial vector ($a_f$) couplings of the $Z$ to the fermions by:

$$A_{\mathrm{FB}}^{\mathrm{f\bar{f}}} = \frac{3}{4}\mathcal{A}_e\mathcal{A}_f = \frac{3}{4}\frac{2a_e v_e}{a_e^2+v_e^2}\frac{2a_f v_f}{a_f^2+v_f^2} \tag{2}$$

Higher order electroweak corrections can be accounted for in the above relations by defining the modified couplings $\bar{v_f}$ and $\bar{a_f}$ and an effective value $\sin^2\theta^{\mathrm{f}}_{\mathrm{W,eff}}$ of the Weinberg mixing angle:

$$\frac{\bar{v_f}}{\bar{a_f}} = 1 - 4\,|q_f|\sin^2\theta^{\mathrm{f}}_{\mathrm{W,eff}} \tag{3}$$

where $q_f$ is the electric charge of the fermion in unit of the proton charge. The effective value of the Weinberg mixing angle quoted is the one corresponding to lepton ($\sin^2\theta^{lept}_{\mathrm{W,eff}}$ ), small contribution specific to the quark sector being corrected for.
Because of the values of the $Z$ couplings to fermions, both the forward-backward asymmetry and its sensitivity to $\sin^2\theta^{lept}_{\mathrm{W,eff}}$ are larger in the $Z \rightarrow q\overline{q}$ channel, thus making the $A_{\mathrm{FB}}^{\mathrm{b\bar{b}}}$ and $A_{\mathrm{FB}}^{\mathrm{c\bar{c}}}$ measurements of particular interest.
The determination of the observed asymmetries $A_{\mathrm{FB}}^{\mathrm{b\bar{b}}}$ and $A_{\mathrm{FB}}^{\mathrm{c\bar{c}}}$ requires:

- the tagging of the hadronic decays of the $Z$ boson into heavy quark final states, $b\bar{b}$ and $c\bar{c}$;
- the reconstruction of the polar angle of the produced quark/anti-quark
- the orientation of the corresponding axis as a function of the quark direction.

The analysis presented here is based on events with identified muons or electrons produced in semileptonic decays of $b$ and $c$ hadrons, shortly referred to as "lepton sample" in the following. The main informations available in these events are:

- the kinematic variables associated with the lepton, namely the transverse ($p_T$) and longitudinal ($p_L$) momentum with respect to the direction of the closest jet;
- the electric charge of the lepton.

Prompt leptons with high $p_T$ and $p_L$ allow to select a high purity sample of $e^+e^- \rightarrow Z \rightarrow b\overline{b}$ events and, at the same time, to discriminate between quark and anti-quark jets on the basis of the charge correlation between the lepton and the parent quark. Decay chains like $b \rightarrow c \rightarrow l^+$ and $B\bar{B}^0$ mixing reduce this charge correlation. Conversely the presence of background and the reduced charge correlations limit the use of the largest fraction of the lepton sample at low $p_T$ and $p_L$. Two additional variables were used in the present analysis to overcome these limitations in the $A_{\mathrm{FB}}^{\mathrm{b\bar{b}}}$ measurement :

- a b-tagging variable, mainly based on the compatibility of the impact parameter of the event tracks with the primary vertex, to isolate pure samples of $e^+e^- \rightarrow Z \rightarrow b\bar{b}$ events;

- a momentum weighted average of the particle charges in the hemisphere opposite to the lepton, to provide an independent estimator of the charge of the primary quark.

By combining the information from the b-tagging and the lepton $p_L$ and $p_T$, a clean sample of $Z \rightarrow c\bar{c}$ could be selected, thus allowing also the measurement of $A_{\rm FB}^{\rm c\bar{c}}$ .

The thrust axis of the event, oriented by the jet containing the lepton, was used to determine the direction of the primary quark.

The data used here were collected between 1993 and 1995 at energies around the $Z$ peak with the DELPHI detector at LEP. This analysis extends the previously published results based on the events collected in 1990 [1], 1991 and 1992 [2].

After a brief presentation of the DELPHI detector, the event and lepton selections are described, the observables used in the analysis are discussed together with their correct description by the simulation and the associated sources of systematics and then measurement of the asymmetries $A_{\rm FB}^{\rm b\bar{b}}$ and $A_{\rm FB}^{\rm c\bar{c}}$ is presented.

# 2 Detector description and event selection

## 2.1 The DELPHI detector

The DELPHI detector has been described in detail in [3]. Only the components more relevant to the analysis are discussed here.

The tracking of charged particles was accomplished with a set of cylindrical tracking detectors with the axis oriented along the 1.23 T magnetic field and the direction of the beam.

The innermost detector in DELPHI was the Vertex Detector (VD), located just outside the LEP beam pipe. It consisted of three concentric layers of silicon microstrip detectors at average radii of 6.3, 9.0 and 10.9 cm from the beam line, called the Closer, Inner and Outer layer, respectively. Until 1993 it provided only the measurement of the $R\Phi$ [1] coordinate and the polar angle acceptance for a particle crossing all the three layers was limited by the extension of the Outer layer to $44^\circ \leq \theta \leq 136^\circ$ [4]. In 1994 the Closer and the Outer layers were equipped with double sided silicon detectors, also measuring the $z$ coordinate [5]. At the same time the angular acceptance of the Closer layer was enlarged from $30^\circ \leq \theta \leq 150^\circ$ to $25^\circ \leq \theta \leq 155^\circ$. The measured intrinsic precision was about 8 $\mu$m for the $R\Phi$ measurement while for $z$ it depended on the polar angle of the incident track, going from about 10 $\mu$m for tracks perpendicular to the modules, to 20 $\mu$m for tracks with a polar angle of $25^\circ$. For charged particle tracks with hits in all three $R\Phi$ VD layers, the impact parameter[2] precision was $\sigma_{R\Phi} = [61/(p\sin^{3/2}\theta) \oplus 20]\mu$m while for tracks with hits in both the $Rz$ layers it was $\sigma_z = [67/(p\sin^{5/2}\theta) \oplus 33]\mu$m, being $p$ the momentum in GeV/$c$.

[1] In the DELPHI coordonate system, $z$ is along the beam line, $\Phi$ and $R$ are the azimutal angle and radius in the $xy$ plane, and $\theta$ is the polar angle with respect to the $z$ axis.

[2] The impact parameter is defined as the distance of closest approach of a charged particle to the reconstructed primary vertex.

Outside the VD, between radii of 12 cm and 28 cm, the Inner Detector (ID) was located, which included a jet chamber providing up to 24 $R\Phi$ measurements and five layers of proportional chambers with both $R\Phi$ and $z$ information. The ID covered the angular range $29^\circ \leq \theta \leq 151^\circ$. In 1995 a new ID was operational, with the same wire configuration in the inner drift chamber but a wider polar angle acceptance $15^\circ \leq \theta \leq 165^\circ$.
The VD and the ID were surrounded by the main DELPHI tracking device, the Time Projection Chamber (TPC), a cylinder of 3 m length, of 30 cm inner radius and of 122 cm outer radius. The ionization charge produced by particles crossing the TPC volume was drifted to the ends of the detector where it was measured in a proportional counter. Up to 16 space points could be measured in the angular region $39^\circ \leq \theta \leq 141^\circ$. The analysis of the pulse height of the signals of up to 192 sense wires of the proportional chambers allowed the determination of the specific energy loss, $dE/dX$, of charged particles used for particle identification.
The Outer Detector (OD) was located between radii of 198 cm and 206 cm and consisted of five layers of drift cells.
In the forward regions two sets of planar wire chambers, at $\pm$ 160 cm and $\pm$ 270 cm in $z$, completed the charged particle reconstruction at low angle.

The muon identification relied mainly on the muon chambers, a set of drift chambers with three-dimensional information situated at the periphery of DELPHI after approximately 1 m of iron. One set of chambers was located 20 cm before the end of the hadronic calorimeter, two further sets of chambers being outside. At $\theta \simeq 90^\circ$ there were 7.5 absorption lengths between the interaction point and the last muon detector.

In the Barrel part of the detector there were three layers each including two active planes of chambers covering the region $|\cos\theta| < 0.63$. The two external layers overlapped in azimuth to avoid dead spaces. In the Forward part, the inner and the outer layers consisted of two planes of drift chambers with anode wires crossed at right angles. The resolution was 1.0 cm in $z$ and 0.2 cm (0.4 cm) in $R\Phi$ for the Barrel (Forward). In 1994 a further set of chambers (Surrounding Muon Chambers) was added to cover the region between the Barrel part and the Endcaps. These last chambers were used only for part of the 1994 data analysis.

The electromagnetic calorimeter in the barrel region, $|\cos\theta| < 0.73$, was the High density Projection Chamber (HPC), situated inside the superconducting coil. The detector had a thickness of 17.5 radiation lengths and consisted of 144 modules arranged in 6 rings along $z$, each module divided into 9 drift layers separated by lead. It provided three-dimensional shower reconstruction. In the forward region, $0.80 < |\cos\theta| < 0.98$, the electromagnetic calorimeter EMF consisted of two disks of 5 m diameter with a total of 9064 lead-glass blocks in the form of truncated pyramids, arranged almost to point towards the interaction region.

## 2.2 Selection of hadronic events

The selection of charged particle tracks and neutral clusters was performed according the requirements of table 1. Hadronic events were then selected requiring:

1. at least 7 accepted charged particles;

2. a total measured energy of these charged particles, assuming pion masses, larger that 0.15 times the center of mass energy, $\sqrt{s}$.

| | | |
|---|---|---|
| charged-particle tracks | polar angle $\lvert\cos\theta\rvert$ | $< 0.93$ |
| | length of track measured inside TPC | $> 30$ cm |
| | impact parameter ($R\Phi$) | $< 5$ cm |
| | impact parameter $\lvert z\rvert$ | $< 10$ cm |
| | charged particle momentum | $> 0.2$ GeV |
| | relative uncertainty on the momentum | $< 100\%$ |
| neutral clusters | detected by HPC or EMF | |
| | polar angle $\lvert\cos\theta\rvert$ | $< 0.98$ |
| | HPC (EMF) energy | $> 0.8(0.4)$ GeV |

Table 1: Cuts used for particle selection

A total of 2.7 million hadronic events was selected from 1993-95 data, at centre-of-mass energies within ± 2 GeV of the Z resonance mass. A set of 8.4 million simulated hadronic events for years 1993 to 1995 was used, generated using JETSET 7.4 Parton Shower model [6] in combination with the full simulation of the DELPHI detector. The parameters of the generator were tuned to the DELPHI data as described in [7]. The detailed breakdown of the events used in data and simulation for each year is given in table 2.

| Year | Data events | Simulation events |
|---|---|---|
| 1993 | 696000 | 2276000 |
| 1994 | 1370000 | 4300000 |
| 1995 | 662400 | 1829000 |

Table 2: The number of selected hadronic events for data and simulation

# 3 Lepton samples

## 3.1 Muon sample

For the muon identification the tracks reconstructed in the central detectors were used to define a path along which hits in the muon chambers were looked for. The identification algorithm has been described extensively in ref. [2]. Muon candidates with a momentum, $p$, above 2.5 GeV/$c$ and in the region of good geometrical acceptance were selected. The muon polar angle $\theta_\mu$ was required to be in the region $0.03 < |\cos\theta_\mu| < 0.6$ or $0.68 < |\cos\theta_\mu| < 0.93$. For a small fraction of the 1994 data sample the Surrounding Muon Chambers, which filled the gap between the barrel and forward detectors, were also used.

The muon identification efficiency was measured in $Z \to \mu^+\mu^-$, $Z \to \tau^+\tau^-$ and $\gamma\gamma \to \mu^+\mu^-$events, yielding on average about 0.85 for 45 GeV/$c$ muons and 2% lower for

| Lepton candidate source | Sample composition in % | |
|---|---|---|
| | $\mu$ | $e$ |
| prompt $b$ lepton "same sign" | 32.5 | 35.1 |
| a) $b \to l^-$ | 29.0 | 31.7 |
| b) $b \to \tau \to l^-$ | 1.0 | 1.0 |
| c) $b \to \bar{c} \to l^-$ ; $b \to \bar{c} \to \tau \to l^-$ | 2.5 | 2.5 |
| other prompt $b$ lepton | 12.1 | 12.0 |
| d) $b \to c \to l^+$ ; $b \to c \to \tau \to l^+$ | 11.8 | 11.7 |
| e) $b \to J/\Psi \to l^+l^-$ | 0.3 | 0.3 |
| prompt $c$ lepton | 16.8 | 15.9 |
| f) $c \to l^+$ ; $c \to \tau \to l^+$ | 16.8 | 15.9 |
| Background | 38.6 | 37.0 |
| g) Miss identification | 26.3 | 18.2 |
| h) Light mesons decay / converted gamma / other | 12.3 | 18.8 |

Table 3: *Full lepton sample composition in %. The total efficiency to select a $\mu$ or $e$ from the process "a)"is respectively* $44.7 \pm 0.2$ *% and* $35.4 \pm 0.4$ *% including all effects (momentum cuts, detector inefficiencies ,...) except the 95% efficiency to select hadronic events.*

momentum between 10 and 5 GeV/$c$ . Corrections of $\sim \pm 1 - 3\%$ were implemented in the simulation.

The sensitivity of the asymmetries to the efficiency is small, but in order to extract $A_{\rm FB}^{\rm b\overline{b}}$ and $A_{\rm FB}^{\rm c\overline{c}}$ from the observed asymmetry a correct description of the fraction of background in the sample is needed. The contamination from misidentified hadrons arises partly from the decay of pions and kaons, but for momentum above 3 GeV/$c$ mostly from energetic hadrons interacting at the end of the calorimeter and generating punch-through. $K_S^0$ particles decaying into two pions were used to measure the rate of pion misidentification showing that the fraction of misidentified pions was $1.79 \pm 0.09 \pm 0.05$ and $1.41 \pm 0.10 \pm 0.03$ times bigger in the data than in the simulation, for the barrel and the forward region, respectively. The first error is due to the limited statistics, the second to a 15% change in the amount of muons from pion decays.

To further study the sample composition directly from the data the number of muon candidates normalised to the number of hadronic $Z$ decays, was compared between data and simulation in samples enriched in prompt muons or background by different sets of selections in $p$, $p_T$ or b-tagging. The corrections obtained with these different approaches were found to be compatible. The b-tagging technique, which provided the best statistical precision in the barrel, was used to control the stability of the efficiency and background corrections as a function of $p$ and $p_T$. For the measurements of the $A_{\rm FB}^{\rm b\overline{b}}$ and $A_{\rm FB}^{\rm c\overline{c}}$ the background estimation was based on the $K_S^0$ sample results, with an error of 6% and 8% for the barrel and forward region respectively, independent of the b-tagging.

The rate of muons from $\pi$ and $K$ decays was studied with the same tools. In order to get a sample enriched in $\mu$ of such origin , muon candidates were selected with a momentum down to 2.5 GeV/$c$ , instead of the 3 GeV/$c$ requirement used for the study of the misidentified muons. A good agreement between data and simulation was found within a statistical error of 15% on the number of muon candidates from light hadron

decays.

The comparison between the data and the simulation for the $\cos\theta_\mu$ distribution is presented in figure 1. The $\mu$ sample composition is given table 3.

## 3.2 Electron sample

The electron candidates were identified in the barrel ($0.03 < |\cos\theta_e| < 0.7$ ) by combining the electromagnetic shower information from the HPC and the track ionization measured by the TPC, with a neural network. In the forward region ($0.7 < |\cos\theta_e| < 0.9$) only the ionization measured by the TPC was used.

To control better the detector acceptance and the background level, candidates were selected with $p > 2$ GeV/$c$ .

### Electron in the barrel

A study of electrons from Compton scattering and photon conversion samples showed that the efficiency was lower in the data than in the simulation by about 10% in the barrel. Because of the sensitivity of the electron identification to the density of tracks in the event, the efficiency obtained with low multiplicity samples (compton) or high track density samples (converted photons) could not be extrapolated in a straightforward way to any hadronic events as done in the muon case. As in the muon case, a study based on b-tagging could be used instead to estimate the efficiency and contamination of the electron sample directly in the data sample. The efficiency correction found with the b-tagging was lower but, within 1.5 standard deviation, compatible with the estimation made with the special samples. The same b-tagging analysis measured a misidentification probability in the data 0.9 lower than in the simulation , with variations within a few percent as a function of the year and the angular region considered. The precision on this correction was estimated to be 5%. The selection of enriched samples based on $p$, $p_T$ requirements gave compatible results.

For the measurement of the $A_{\rm FB}^{\rm b\overline{b}}$ and $A_{\rm FB}^{\rm c\overline{c}}$ the numbers obtained with the b-tagging analysis were used to correct the simulation, ending to an error of 5% on the contamination from hadrons and 10% on the contamination from converted photons.

### Electron in the Forward

In the forward region, where only the ionization measured by the TPC was used, the misidentification could be studied with the muon sample itself, $\mu$ and $\pi$ having almost the same ionization signature in the TPC. This showed an underestimation of the misidentification in the simulation by a factor $1.12 \pm 0.07$ . The amount of electron from converted photons was controlled with the help of the b tagging and $p$, $p_T$ requirements. This amount was found to be correctly described for the different years within a precision better than 10%.

The comparison between the data and the simulation for the $\cos\theta_e$ distribution is presented in figure 2. The electron sample composition is quoted table 3.

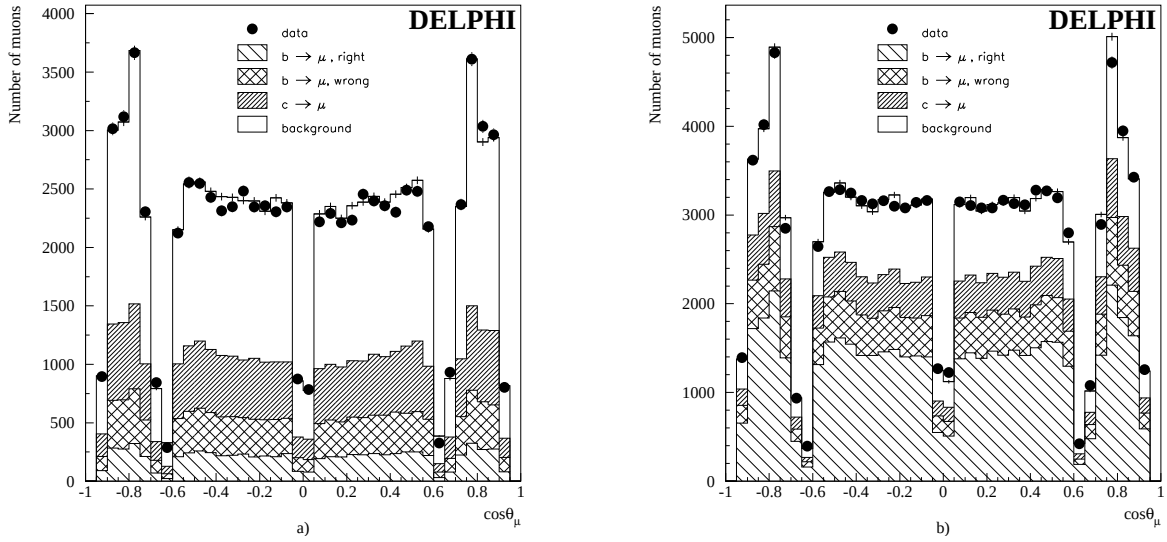


Figure 1: $\cos\theta_\mu$ *distribution for muon candidates. The muons candidate have* $p_T < 0.7$ GeV/$c$ *in a) and* $p_T > 0.7$ GeV/$c$ *in b) correponding to sample enriched, respectively, in background or signal.*

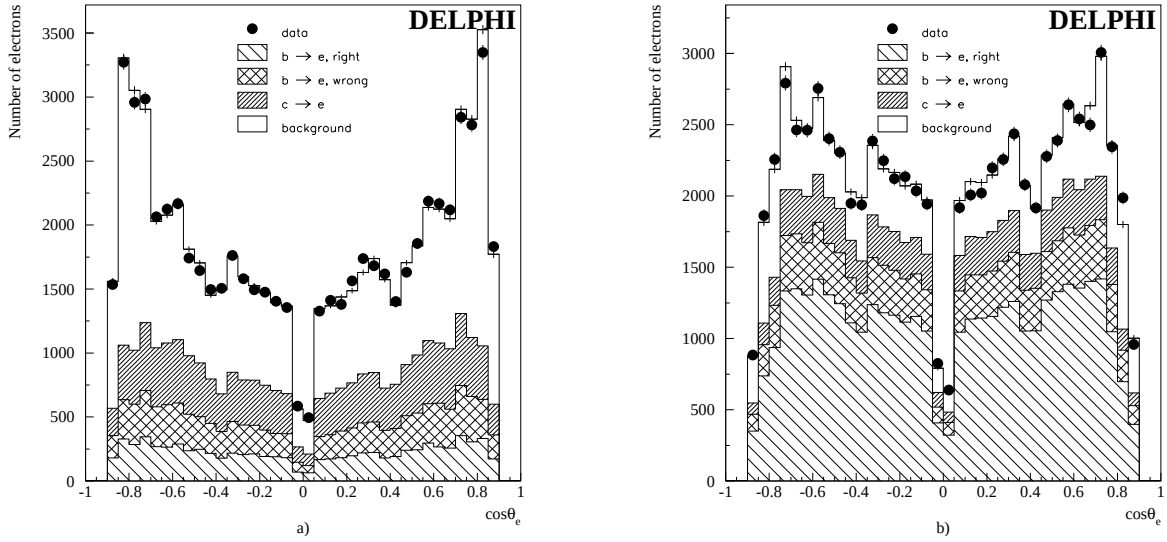


Figure 2: $\cos\theta_e$ *distribution for electron candidates. The electrons candidate have* $p_T < 0.7$ *GeV/c in a) and* $p_T > 0.7$ *GeV/c in b) correponding to sample enriched, respectively, in background or signal. The electrons from converted gamma are at the origin of the strong* $\cos\theta_e$ *dependance of the background in a).*

| Year | Energy | Number of $\mu$ | Number of $e$ |
|---|---|---|---|
| 1993 | 89 GeV | 6070 | 4240 |
| | 91 GeV | 28800 | 21500 |
| | 93 GeV | 9170 | 6540 |
| 1994 | 91 GeV | 95200 | 70000 |
| 1995 | 89 GeV | 5150 | 4060 |
| | 91 GeV | 28600 | 21800 |
| | 93 GeV | 8630 | 6440 |

Table 4: *Number of lepton candidates for the different years and for the three center of mass energies.*

### 3.3 Lepton for the asymmetries measurement

The main kinematical variable used to measure the flavour composition of the leptonic sample was the transverse momentum, $p_T$, of the lepton with respect to the closest jet, the lepton being excluded from the jet. Jets were reconstructed using the JADE algorithm [8] with a scaled invariant mass $y_{cut} = \frac{m_{ij}^2}{E_{vis}^2} \geq 0.01$ .

To ensure a good determination of the jet and thrust polar angle ($\theta_T$), the analysis was limited to events with $\cos(\theta_T) < 0.9$. Events with more than one lepton candidate were used only once. In events with more than one lepton, only the lepton with the highest $p_T$ was considered.

The repartition of the lepton candidates in function of the different years and center of mass energies can be found table 4.

## 4 Use of the $b$-tagging

To improve the separation between heavy and light flavours a $b$-tagging technique developed for the measurement of $R_b$, the partial width of $Z$ into $b\bar{b}$ pairs, was used [9]. Each event was divided into two hemispheres according to the direction of the thrust axis, and the probability for a hemisphere to include a $b$ quark was given by the jet with the highest probability in the hemisphere itself.

The tagging technique was based on the combination of four different discriminating variables ($x_i = 1, 4$) defined for each jet:

- the jet lifetime probability, constructed from the positively signed impact parameters of all the tracks included in a jet, and corresponding to the probability of all those tracks compatible with originating at the primary vertex;
- the effective mass of the particles included in the secondary vertex [3];

[3] A secondary vertex was required to contain at least 2 tracks not compatible with the primary vertex and to have $L/\sigma_L > 4$ where $L$ is the distance from the primary to the secondary vertex and $\sigma_L$ is its error. Each track included in the secondary vertex should have at least one measurement in the VD and at least 2 tracks should have measurements in both $R - \Phi$ and the $R - z$ planes of the VD.

- the rapidity of tracks included in the secondary vertex with respect to the jet direction;
- the fraction of the charged energy of a jet included in the secondary vertex.

In each hemisphere, the four variables $x_i$ were then combined into a single tagging variable $y$ by means of their probability density functions $f_i^q(x_i)$, $f_i^c(x_i)$, $f_i^b(x_i)$, for $uds$, $c$ and $b$ quarks, respectively:

$$y = n_c \prod \frac{f_i^c(x_i)}{f_i^b(x_i)} + n_q \prod \frac{f_i^q(x_i)}{f_i^b(x_i)}$$

being $n_c$, $n_q$ the number of $c$-jets and $uds$-jets with a reconstructed secondary vertex normalized by the relation: $n_c + n_q = 1$. Only the first variable was used if no secondary vertex was reconstructed. Hemispheres with a jet containing a b-quark were characterised by a large value of the variable $\eta_{HEM} = -\log_{10} y$.

In order to maximize the efficiency of the tagging in the high b purity region, the probability for an event to be a $Z \to b\bar{b}$ decay was computed from the hemisphere probabilities as:

$$\eta_{EVT} = \max(\eta_{HEM1}, \eta_{HEM2})$$

The knowledge of the sample composition as a function of $\eta_{EVT}$ was needed to extract $A_{\rm FB}^{\rm b\bar{b}}$ and $A_{\rm FB}^{\rm c\bar{c}}$ from the observed asymmetries. Since a separate tag for each hemisphere was used, the sample composition could be derived from the data themselves with a minimum input from the simulation by using a technique similar to the single tag versus double tag method of the $R_b$ analysis [9].

For events with the thrust axis in the barrel ($|\cos\theta_T| < 0.7$), the distribution of the hemisphere $b$-tagging variable $\eta_{HEM}$ was divided into three intervals, enriched in $uds$ (I), $c$ (II) or $b$ (III) content respectively. In each interval $j$ the fraction $f_E^{(j)}$ of events with at least one hemisphere in that interval and the fraction $f_H^{(j)}$ of hemispheres in the interval itself, were expressed by the following relations:

$$\begin{aligned} f_E^{(j)} &= \sum_{q=uds,c,b} r_q \varepsilon_q^{(j)} \left[2 - \rho_q^{(j)} - \varepsilon_q^{(j)}(1 - \rho_q^{(j)})\right] \\ f_H^{(j)} &= \sum_{q=uds,c,b} r_q \varepsilon_q^{(j)} \end{aligned} \tag{4}$$

where $\varepsilon_q^{(j)}$ were the fractions of hemispheres in the $j-$th interval for the flavour $q$ ($q = uds, c, b$), and the correlations $\rho_q^{(j)}$ accounted for the probability of having both hemispheres in that interval.
In contrast to the $R_b$ analysis, where the selection of the hadronic events was only slightly biasing the flavour composition of the sample, in this analysis the requirement of an identified lepton in the final state strongly enhanced the fraction of events with a $Z$ decaying into heavy quark pairs. Therefore the fractions $r_q$ of $Z \to q\bar{q}$ events in the selected leptonic sample were obtained from $R_q$, the Standard Model partial decay widths of the $Z$, via the relation

$$r_q = R_q \frac{e_{q,\ell}}{e_{had,\ell}} \quad q = uds, c, b \tag{5}$$

where $e_{q,\ell}$ was the flavour dependent hadronic selection efficiency, taken from the simulation, and $e_{had,\ell} = \sum_{uds,c,b} e_{q,\ell}$.

The set of equations (4) for different intervals were not independent as for each flavour $q$ the $\varepsilon_q^{(j)}$ had to satisfy the closure relation:

$$\sum_{j}^{N_{int}} \varepsilon_q^{(j)} = 1 \tag{6}$$

with the sum running over the $N_{int} = 3$ intervals.
To solve the system formed by the $2 \times N_{int}$ equations (4) and the 3 constraints (6), a first order expansion of the efficiencies in the data $\varepsilon_{q,RD}^{(j)}$ as a function of the ones in the simulation, $\varepsilon_q^{(j)}$, was performed:

$$\varepsilon_{q,RD}^{(j)} = \varepsilon_q^{(j)}(1 + \delta_q^{(j)})$$

In the approximation, confirmed by the data, of small corrections $\delta_q^{(j)}$ equations 4 and 6 yield:

$$\begin{aligned}
\sum_{q=uds,c,b} r_q \varepsilon_q^{(j)} \left[2 - \rho_q^{(j)} - 2\varepsilon_q^{(j)}(1 - \rho_q^{(j)})\right] \delta_q^{(j)} &= f_E^{(j)} - \sum_{q=uds,c,b} r_q \varepsilon_q^{(j)} \left[2 - \rho_q^{(j)} - \varepsilon_q^{(j)}(1 - \rho_q^{(j)})\right] \\
\sum_{q=uds,c,b} r_q \varepsilon_q^{(j)} \delta_q^{(j)} &= f_H^{(j)} - \sum_{q=uds,c,b} r_q \varepsilon_q^{(j)} \\
\sum_{q=uds,c,b} \varepsilon_q^{(j)} \delta_q^{(j)} &= 0
\end{aligned}$$

where $\rho_q^{(j)}$ and $\varepsilon_q^{(j)}$ were taken from the simulation. For $N_{int} = 3$ there were in total 9 unknowns $\delta_q^{(j)}$ and 9 equations. The rank of the matrix of the coefficients was 8 so that one input efficiency was required. For $N_{int} = 2$ the system reduced to 6 equations. Merging together the efficiencies for 2 flavours the number of unknowns reduced to 4. Since the rank of the matrix of the coefficients was 4 the system had one exact solution. Therefore the $\delta_q^{(j)}$ for $N_{int} = 3$ were obtained in two steps. First we combined together the two highest bins of $\eta_{HEM}$ , merged the $c$ and $b$ contributions and solved this reduced system with 4 equations. After the full system was solved fixing $\delta_{uds}^{(I)}$ to the value obtained in the previous step.

In the case of events with $0.7 < |\cos\theta_T| < 0.85$, because of the reduced performances of $b$-tagging in the forward region, only the reduced system with 4 equations was solved. No $b$-tagging information was used for events with $|\cos\theta_T| > 0.85$ [4].

The errors on the $\delta_q^{(j)}$ due to the finite statistics of the simulated sample were estimated in the following way. For each flavour $q$, we considered all the two dimensional distributions $\{\eta_{HEM1}, \eta_{HEM2}\}$ which could be derived from the original one in the simulation by adding -1, 0, and +1 standard deviations to the content of each interval. This

[4]For the 1993 data sample due to the reduced length of the micro-vertex detector, the $b$-tagging was performed only down to $|\cos\theta_T| < 0.81$

was done conserving the total number of the events of that flavour and with the standard deviations given by multinomial distribution. For each configuration the coefficients $\varepsilon_q^{(j)}$, $\rho_q^{(j)}$ in Eq. 6 were recomputed and then the system solved. The spread of the different solutions for the $\delta_q^{(j)}$ was considered as the simulation statistical error on these corrections. As a cross check of the method, the simulated sample was divided into 6 different sub-samples of equal size. For each sub-sample, the system was solved and the uncertainty on the solutions was evaluated by using the procedure described above. The spread of the solutions in the subsets was found to be in agreement with the estimation of the error. The corrections $1+\delta_q^{(j)}$ to the simulation efficiencies found for the 1994 sample together with the error due to the finite simulation statistics are shown in Table 5. For all the samples the corrections $\delta_{uds}^{(III)}$ were found to be compatible with zero indicating a good control of the background level in the region most relevant to this measurement. The efficiencies $\varepsilon_b^{(III)}$ were found instead 2-4 % higher in the data than in the simulation.

| bin | I | II | III |
|---|---|---|---|
| (dominant flavour) | ($uds$) | ($c$) | ($b$) |
| Barrel | | | |
| $\varepsilon_{uds}^{(j)}$ | .71 | .23 | .06 |
| $1+\delta_{uds}^{(j)}$ | 1.019 ± 0.003 | 0.950 ±0.017 | 0.986 ± 0.072 |
| $\varepsilon_c^{(j)}$ | .45 | .34 | .21 |
| $1+\delta_c^{(j)}$ | 0.986 ± 0.007 | 1.046 ± 0.013 | 0.956 ± 0.031 |
| $\varepsilon_b^{(j)}$ | .13 | .18 | .69 |
| $1+\delta_b^{(j)}$ | 0.970 ± 0.009 | 0.946 ± 0.006 | 1.020 ± 0.002 |
| Forward | | | |
| $\varepsilon_{uds}^{(j)}$ | .70 | .30 | |
| $1+\delta_{uds}^{(j)}$ | 1.000 ± 0.009 | 1.000 ± 0.021 | |
| $\varepsilon_{bc}^{(j)}$ | .36 | .64 | |
| $1+\delta_{bc}^{(j)}$ | .931 ± 0.008 | 1.039 ± .005 | |

Table 5: Simulation efficiencies $\varepsilon_q^{(j)}$ and their corrections $1+\delta_q^{(j)}$ to describe the 1994 data sample with the errors due to the finite simulation statistics.

For the system with $N_{int}=3$ the predicted correlations have a sizeable value only for $\rho_b^{(III)}$ ( $=0.027\pm0.005$ in 1994 ). The detector and QCD origines of such correlation have been studied in detail in [9]. In the present analysis even a 100% change in the predicted correlation has a small impact on the estimated data sample composition. The variation induced is of the same order than the one associated to the statistical uncertainty on $\delta_q^{(j)}$.

For the system with $N_{int}=2$ the predicted correlations were up to $\sim 0.1$ for the $b/c$ flavours and still compatible with zero for $uds$ sample. The high value of $\rho_{bc}^{(j)}$ in this case is a pure artefact of the merging of the $b$ and $c$ samples and is just related, at first order, to the difference in tagging efficiency of $b$ and $c$.

The merging of $b$ and $c$ for $N_{int}=2$ is justified by the fact that for the $b$-tagging intervals used in this case, the efficiency corrections are mainly related to the difference in the description of the detector response between real data and simulation and not to

the details of the $b$ and $c$ physics.

This is supported by the fact that in the interval $I$ dominated by $uds$, which is the same both for $N_{int} = 2$ and $N_{int} = 3$, the corrections $\delta_c^{(I)}$ and $\delta_b^{(I)}$ in the barrel are compatible (cf. Table 5). To evaluate possible biases from this merging procedure, a different system, always with $N_{int} = 2$, was built starting from the original one with $N_{int} = 3$ but now combining the two lowest bins of $\eta_{HEM}$, bins I and II, and merging the $uds$ and $c$ flavours. The changes found on $A_{\rm FB}^{\rm b\bar{b}}$ and $A_{\rm FB}^{\rm c\bar{c}}$ were taken conservatively as systematic errors (cf. section 7).

# 5 Use of the jet charge.

The correlation between the electric charge of the lepton and the flavour of the parent $b$ quark is strong in the region of high longitudinal ($p_L$) and transverse ($p_T$) momentum of the lepton with respect to the closest jet. Nevertheless, the use of the b-tagging allowed for a strong reduction of background events in the lepton sample. Therefore, in this analysis also the region of low $p_L$ and $p_T$ became relevant for the $A_{\rm FB}^{\rm b\bar{b}}$ measurement, provided a clear tagging of right sign ($b \to \ell^-$) and wrong sign ($b \to \ell^+$) leptons is achieved. This tagging is important also in the high $p_L$, $p_T$ region, because $B^0\bar{B}^0$ oscillations produce wrong sign leptons. The goal of determining the flavour of the parent $b$ quark on the basis of the information present in both hemispheres was reached by means of a momentum-weighted ($p_i$) average of the charges ($q_i$) of the particles in the hemisphere opposite to the lepton, referred in the following text as jet charge:

$$Q_{opp} = \frac{\sum_{hem} q_i |\overrightarrow{p_i} \cdot \overrightarrow{T}|^K}{\sum_{hem} |\overrightarrow{p_i} \cdot \overrightarrow{T}|^K}$$

with the event divided into 2 hemispheres by a plane perpendicular to the thrust axis $\overrightarrow{T}$.

In this definition the information coming from the tracks in the lepton hemisphere were not used in order to avoid the strong bias in the topology due to the presence of a lepton. Based on the work presented in [10] $K = 0.8$ was chosen to optimize the $b/\bar{b}$ separation. We restricted the use of the jet charge to the events with the thrust axis in the barrel ( $|\cos\theta_T| < 0.7$) belonging to the lepton subsample enriched in b (bin III according to the definition given in section 4).

The distribution of the total event jet charge in the hadronic decays of the $Z$ turned out to be systematically displaced from zero ($\sim +0.01$), due to the hadronic interactions of the particles inside the detector. We checked that this shift was independent of the event flavour in each $b$-tag bin and corrected for it, separately in the data and in the simulation, by using a function of the thrust axis of the event. After this correction it was possible to treat in a consistent way positive and negative leptons, by using, as $b/\bar{b}$ discriminating variable, the product of the lepton charge times the jet charge, $Q_\ell \times Q_{opp}$. For a pure sample of leptons coming from $Z \to b\bar{b}$ decays, $Q_\ell \times Q_{opp}$ has a gaussian distribution centred at negative (positive) values in case of right (wrong) sign leptons. In the following we refer to this central value as $\pm m$ and to the width of the gaussian as $\sigma$.

The use of the jet charge as as $b/\bar{b}$ discriminating variable increased substantially the statistical precision of the $A_{\rm FB}^{\rm b\bar{b}}$ measurement. Furthermore a procedure of self-calibration of the jet charge on the data allowed the fraction $f$ of right sign leptons to be more independent of the simulation, thus reducing considerably the systematic dependence on

the $B^0\bar{B}^0$ mixing and on the branching fractions for the direct ($b \to \ell$) and cascade ($b \to c \to \ell$) semileptonic decays.

The first step of the jet charge self calibration consisted in the tuning of the distribution in the simulation in order to reproduce correctly in the data the total jet charge of the event. For this purpose the overall sample of b-tagged hadronic $Z$ decays could be used, thus getting a small statistical uncertainty.

As a second step the values of $f$, $m$ were fitted from the distribution in the data of $Q_\ell \times Q_{opp}$. This has been done for each year for $\mu$ and $e$ separately, after subtracting the background predicted by the simulation. The statistical sensitivity of the fit was improved by using the relation

$$< Q_\ell \times Q_{opp} >= (1 - 2f)m \tag{7}$$

to reduce the number of fitted parameters.
Subsequently the jet charge distribution in the simulation was rescaled according to the measured values of $m$, $\sigma$ and, in each lepton subsample, the events were reweighted in order to reproduce the fitted value of right sign leptons $f$. After this calibration the simulation describes correctly the data as can be seen in figure 3.

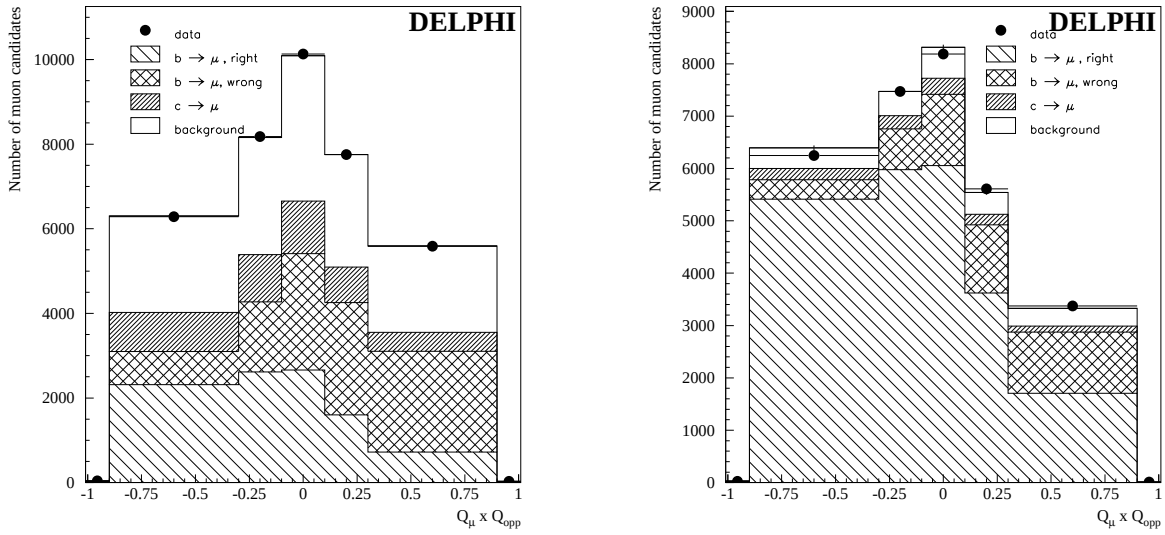


Figure 3: *Jet charge distribution for the full muon sample. The muons candidates have* $p_{Tout} < 1.3$ GeV/$c$ *and* $p < 7$ GeV/$c$ *(left) and* $p_{Tout} > 1.3$ GeV/$c$ *(right) correponding to sample enriched, respectively, in* $b \to c \to \mu^+$ *or* $b \to \mu^-$. *After a tuning of* $Q_\ell \times Q_{opp}$ *on the full sample, the fact than sub-samples with different kind of charge correlation between the lepton and the oposit hemisphere are correctly described is a nice confirmation of the good understanding and description of the lepton sample used in this analysis.*

There are two sources of uncertainty connected with this self calibration of jet charge:

- The measurement of $\sigma$, $f$ and $m$ is done with a given statistical precision (see table 6).
- The $\sigma$ and $m$ values for the background component are taken from simulation. Nevertheless the correct description of these $\sigma$ and $m$ can be estimated using samples enriched in $uds$ or $c$, as defined in section 4.

| | $\sigma$ | $f$ | | $m$ | |
|---|---|---|---|---|---|
| | | $\mu$ sample | $e$ sample | $\mu$ sample | $e$ sample |
| Data | 0.3210 ± 0.0004 | .684 ± .006 | .702 ± .008 | .099 ∓ .003 | .098 ∓ .004 |
| Simulation | 0.3248 ± 0.0003 | .693 ± .004 | .711 ± .004 | .103 ∓ .002 | .101 ∓ .002 |

Table 6: *Values of $\sigma$, $f$ and $m$ in the barrel for the subsample enriched in b, fitted in the data and in the simulation in 1994. It should be noticed that due to equation 7, $f$ and $m$ are fully anti-correlated.*

# 6 The fit of the asymmetries

The $A_{\rm FB}^{\rm b\overline{b}}$ and $A_{\rm FB}^{\rm c\overline{c}}$ asymmetries were extracted from a minimum $\chi^2$ fit to the observed charge asymmetry $A_{FB}^{obs,i}$ defined as:

$$A_{FB}^{obs,i} = \frac{N^-(i) - N^+(i)}{N^-(i) + N^+(i)}$$

where $N^{\pm}(i)$ are the numbers of leptons with $\pm$ sign in the $i$-th bin.
Four variables were used for binning the sample: $\cos\theta_T$, which accounted for the polar angle dependence of the asymmetries, and 3 multivariate classification parameters, defined to have bins enriched with leptons from a single origin in order to reduce the statistical errors of the $A_{\rm FB}^{\rm b\overline{b}}$ and $A_{\rm FB}^{\rm c\overline{c}}$ measurements.

## 6.1 The multivariate parameters

The observables entering the multivariate parameters for classifying the lepton candidates as a function of their origin were chosen to be:

- the transverse ($p_T$) and longitudinal ($p_L$) momenta of the lepton;
- the event b-tagging, $\eta_{EVT}$;
- the product of the lepton charge times the jet charge of the opposite hemisphere, $Q_\ell \times Q_{opp}$.

The choice of these variables was determined by the capability of calibrating them on the data, reaching in this way a good control of the systematics.

Starting from these observables a multivariate tagging of the lepton origin was built by considering four multivariate classes:

1. $b_r$ : leptons from $b$ decays in $Z \to b\bar{b}$ events with the right sign correlation with respect to the primary quark;
2. $b_w$ : leptons from $b$ decays in $Z \to b\bar{b}$ events with the wrong sign correlation with respect to the primary quark;
3. $c$ : prompt leptons from $c$ decays in $Z \to c\bar{c}$;

4. *bkg* : other processes (misidentified hadrons, muons and electrons from light hadron decay, electrons from photon conversions and leptons from heavy flavours coming from a gluon splitting).

The sign correlation previously mentioned refers to the one between the lepton charge and the $b/\bar{b}$ flavour at production and therefore it includes possible effects due to $B\bar{B}$ mixing (cf. section 6.3 for a more extended discussion on the mixing). The probabilities $p_k^{p_T,p_L}$ and $p_k^{btag,jet-ch}$ of observing a set of $(p_T, p_L)$ and ($\eta_{EVT}$, $Q_\ell \times Q_{opp}$) values for a lepton from the multivariate class $k$ were computed by using two dimensional distributions from the tuned simulation. A likelihood ratio $\mathcal{P}_k$ was built to estimate the probability corresponding to a given set of values within a given class:

$$\mathcal{P}_k = \frac{N_k p_k^{p_T,p_L} p_k^{btag,jet-ch}}{\Sigma_{k'} N_{k'} p_{k'}^{p_T,p_L} p_{k'}^{btag,jet-ch}}$$

where $N_k$ ($N_{k'}$) is the total number of leptons from the multivariate class $k$ ($k'$). The scaling in function of $N_k$ in the likelihood ratio, allowed to take into account the relative weights of each class. Neglecting some of the correlations between the observables, such definition identify $\mathcal{P}_k$ as the fraction of lepton candidates with a given set of $p_T, p_L, \eta_{EVT}$ and $Q_\ell \times Q_{opp}$ belonging to the class $k$.

This technique, used for the multivariate classification, extends that in [9] by considering probabilities in two dimensions. Thus it takes into account part of the correlations between pairs of observables by construction.
In order to consider possible improvement by taking into account all possible correlations, an approach based on neural network classification was also tried. The obtained results were in good agreement with the multivariate approach with a slightly worse statistical precision. The multivariate approach was chosen as it allowed, for the small number of observables used, a simpler control of the analysis and an optimal use of the available data and simulation statistics.

Out of the four $\mathcal{P}_k$, calculated for each event, only three ($\mathcal{P}_{b_r}, \mathcal{P}_{b_w}$ and $\mathcal{P}_c$) were kept for the $\chi^2$ fit. The corresponding distributions for $\mu$ and $e$ can be found in figure 4.

To take advantage of the opposite sign in the contribution of the $b_r$ and $b_w$ classes to the $b$ asymmetry, the bins for the $\chi^2$ fit were defined by using the combined variable $\mathcal{P}_{b_r} - \mathcal{P}_{b_w}$ and $\mathcal{P}_c$.

## 6.2 Measurement of $A_{\rm FB}^{\rm b\bar{b}}$ and $A_{\rm FB}^{\rm c\bar{c}}$

The asymmetries $A_{\rm FB}^{\rm b\bar{b}}$ and $A_{\rm FB}^{\rm c\bar{c}}$ were extracted from a $\chi^2$ fit to the observed asymmetry $A_{FB}^{obs,i}$ over the different bins of the ($\cos\theta_T$, $\mathcal{P}_{b_r}$-$\mathcal{P}_{b_w}$, $\mathcal{P}_c$ ) parameter space:

$$\chi^2 = \sum_i \frac{\left(\left(\left(f_{b_r}^i - f_{b_w}^i\right) A_{\rm FB}^{\rm b\bar{b}} + f_c^i A_{\rm FB}^{\rm c\bar{c}} + f_{bkg}^i A_{FB}^{bkg,i}\right) W_{\theta_T}^i - A_{FB}^{obs,i}\right)^2}{\sigma_i^2} \tag{8}$$

where :

- $W_{\theta_T}^i = \frac{8}{3}\frac{1}{N_{data}^i}\sum_{j=1}^{N_{data}^i} \frac{\cos\theta_T^j}{1+(\cos\theta_T^j)^2}$ takes into account the dependence of the asymmetry on the polar angle;
- $\sigma_i$ is the statistical error including contributions of both data and simulation;

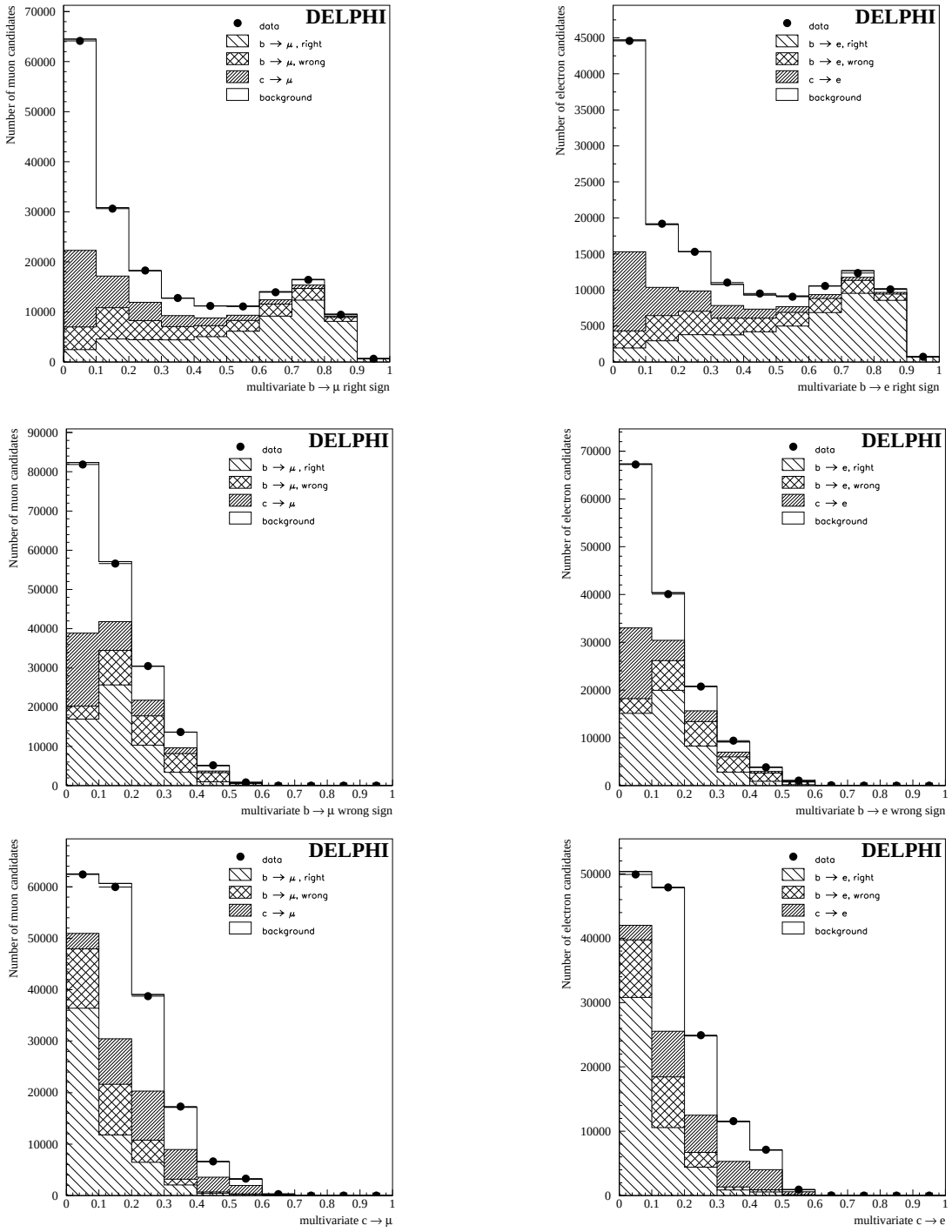


Figure 4: *$\mathcal{P}_{b_r}$ (up) , $\mathcal{P}_{b_w}$ (middle) and $\mathcal{P}_c$ (bottom) distributions for muon (left) and electron (right) for all years.*

- $f_k^i$ are the different fractions in each bin determined from the tuned simulation. [5]

Sign correlation between the lepton candidate and the parent quark can exist also for the misidentified leptons thus leading to non zero values for the background asymmetry $A_{FB}^{bkg,i}$. Furthermore, since this correlation increases with the track momentum and in function of b-tagging value, $A_{FB}^{bkg,i}$ must be known in each bin. To optimize the statistical precision of the estimated $A_{FB}^{bkg,i}$, the same factorisation technique as in the previous analysis [2] was adopted: the simulation was only used to determine the charge correlation between the background and the initial quark in each bin, while the quark asymmetries were set to their Standard Model expectation[6] or to the fited parameters $A_{\rm FB}^{\rm b\overline{b}}$ / $A_{\rm FB}^{\rm c\overline{c}}$ for the background in $b$ / $c$ events.

## 6.3 Effect of the $B\bar{B}$ mixing

The $B\bar{B}$ mixing reduces the charge correlation between the initial $b/\bar{b}$ produced in the $Z$ decay and the lepton produced in the semi-leptonic decay of the $B$ hadron. The size of the change depends on the proper decay time of the $B$ hadron and of its type, resulting in different values of the effective mixing in the different bins of the lepton sample, for the following reasons:

- the $B_d^0$ and $B_s^0$ contents in the $b$ sample are not the same when the decay chain $b \to c \to l^+$ is considered instead of $b \to l^-$, due to differences in the $D^+/D^0/D_s$ production rate by the different B hadrons. This introduces a variation of the effective mixing in function of the amount of $b \to c \to l^+$ compared to $b \to l^-$ which depends, for example, on the $p_T$;

- the use of the b-tagging biases the content of the bins in term of proper decay time, thus introducing sizeable changes in the effective mixing;

- the correlation between the lepton and the jet charge of the opposite hemisphere is directly a function of the mixing.

At present the $B\bar{B}$ mixing is known with a good precision. Following the approach developed in the LEP oscillation working group [11], the simulation was tuned to reproduce the measured $B$ fraction ( $f_{B^\pm}$ , $f_{B_d^0}$, $f_{B_s^0}$ ,$f_{B_{baryon}}$ ) and the time dependence of the oscillations ( $\Delta m_{B_d^0}$ and $\Delta m_{B_s^0}$ ). The values and the corresponding uncertainties used to implement the $B\bar{B}$ mixing in the simulation are listed in table 7. [7]

With this approach, the value estimated from the tuned simulation of $f_{b_r}^i$ and $f_{b_w}^i$ included the expected amount of mixing.

[5] Even if they are almost equal, the meaning of $f_k$ and $\mathcal{P}_k$ is quite different. $\mathcal{P}_k$ is build from observables in data and $f_k^i$ is the sample composition for a given sub-sample, $i$, estimated from a tuned simulation.

[6] The unknown from the exact knowledge of these asymmetries is negligible compared to the error on the charge correlation itself.

[7] The values used come from the LEP Lifetime Working group (lifetimes), the LEP oscillation working group (fractions , $\Delta m_d$ and $\Delta m_s$) and the LEP Heavy Flavour working group ($\chi$). The upper bound value quoted for $\Delta m_s$ was used ($\Delta m_s > 10.6\ ps^{-1}$), no sensitivity to the exact value of this parameter in the allowed domain has been observed. All these numbers are taken from [12].

## 6.4 Results

The measured asymmetries and the corresponding statistical errors using the 1993-1995 lepton samples are listed below:

At $\sqrt{s} = 89.43$ GeV :

$$A_{FB}^{b\bar{b}} = 0.066 \pm 0.022(stat)$$

$$A_{FB}^{c\bar{c}} = 0.030 \pm 0.035(stat)$$

with a correlation of 0.19 and $\frac{\chi^2}{ndf} = \frac{185}{208}$ , Prob($\chi^2$)=0.87,

at $\sqrt{s} = 91.22$ GeV :

$$A_{FB}^{b\bar{b}} = 0.0958 \pm 0.0061(stat)$$

$$A_{FB}^{c\bar{c}} = 0.0585 \pm 0.0098(stat)$$

with a correlation of 0.22 and $\frac{\chi^2}{ndf} = \frac{1416}{1453}$ , Prob($\chi^2$)=0.75,

at $\sqrt{s} = 92.99$ GeV :

$$A_{FB}^{b\bar{b}} = 0.109 \pm 0.018(stat)$$

$$A_{FB}^{c\bar{c}} = 0.108 \pm 0.028(stat)$$

with a correlation of 0.19 and $\frac{\chi^2}{ndf} = \frac{204}{208}$ , Prob($\chi^2$)=0.57.

The result of the fit for a data subsample is presented with the observed asymmetry in figure 5.

To optimize the use of the available statistics , the multivariate variables were computed separately for the different years and lepton samples but all the samples were merged for the $\chi^2$ fit. This allowed to have a reasonable amount of events per bin (respectively $\sim 100$ , $\sim 180$ and $\sim 150$ for $\sqrt{s} = 89.43$ GeV , 91.22 GeV and 92.99 GeV ) with a good sampling in the parameters space.

| Changed parameters | Central value | Variations applied | $\Delta\ A_{\rm FB}^{\rm b\bar{b}}$ Peak | $\Delta\ A_{\rm FB}^{\rm c\bar{c}}$ Peak |
|---|---|---|---|---|
| Lepton Sample | | | **0.0015** | **0.0035** |
| $Br(b \to l)$ | 0.1056 | $\pm$ 0.0026 | $\mp$ 0.00048 | $\pm$ 0.00062 |
| $Br(b \to c \to l)$ | 0.0807 | $\pm$ 0.0034 | $\mp$ 0.00015 | $\mp$ 0.00080 |
| $Br(b \to \bar{c} \to l)$ | 0.0162 | $^{+0.0044}_{-0.0036}$ | $\pm$ 0.00017 | $\pm$ 0.00180 |
| $Br(b \to \tau \to l)$ | 0.00419 | $\pm$ 0.00055 | $\mp$ 0.00001 | $\pm$ 0.00027 |
| $Br(b \to J/\psi \to l)$ | 0.00072 | $\pm$ 0.00006 | $\pm$ 0.00005 | $\pm$ 0.00002 |
| $Br(c \to l)$ | 0.0990 | $\pm$ 0.0037 | $\pm$ 0.00036 | $\mp$ 0.00182 |
| $\Gamma_{b\bar{b}}/\Gamma_{had}$ | 0.21644 | $\pm$ 0.00075 | $\mp$ 0.00007 | $\pm$ 0.00007 |
| $\Gamma_{c\bar{c}}/\Gamma_{had}$ | 0.1671 | $\pm$ 0.0048 | $\pm$ 0.00034 | $\mp$ 0.00130 |
| $g \to b\bar{b}$ | 0.00254 | $\pm$ 0.00051 | $\pm$ 0.00012 | $\pm$ 0.00005 |
| $g \to c\bar{c}$ | 0.0296 | $\pm$ 0.0038 | $\pm$ 0.00012 | $\pm$ 0.00001 |
| $\langle X_E \rangle_B$ | 0.702 | $\pm$ 0.008 | $\mp$ 0.00016 | $\mp$ 0.00019 |
| $\langle X_E \rangle_{D^*}$ in $c\bar{c}$ events | 0.510 | $\pm$ 0.0094 | $\pm$ 0.00047 | $\mp$ 0.00046 |
| $b$ decay model | $ACCMM$ | $^{IGSW}_{IG**}$ | $\mp$ 0.00065 | $\mp$ 0.00111 |
| $c$ decay model | $ALT1$ | $^{ALT2}_{ALT3}$ | $\pm$ 0.00098 | $\mp$ 0.00116 |
| Mixing | | | **0.0010** | **0.0001** |
| $\tau_{B_d}$ | 1.548 ps | $\pm$ 0.032 | $\pm$ 0.00005 | $\pm$ 0.00004 |
| $\tau_{B^\pm}$ | 1.653 ps | $\pm$ 0.028 | $\mp$ 0.00002 | $\mp$ 0.00003 |
| $\tau_{B_s}$ | 1.493 ps | $\pm$ 0.062 | $\mp$ 0.00025 | $\pm$ 0.00001 |
| $\tau_{B_{baryon}}$ | 1.208 ps | $\pm$ 0.051 | $\pm$ 0.00004 | $\mp$ 0.00002 |
| $\langle \tau_{B_{hadron}} \rangle$ | 1.564 ps | $\pm$ 0.014 | $\pm$ 0.00005 | $\pm$ 0.00000 |
| $\tau_{B^\pm}/\tau_{B_d}$ | 1.062 | $\pm$ 0.029 | $\pm$ 0.00016 | $\pm$ 0.00001 |
| $f_{b-baryon}$ | 0.115 | $\pm$ 0.020 | $\mp$ 0.00006 | $\pm$ 0.00010 |
| $f_{B_s}$ | 0.117 | $\pm$ 0.030 | $\pm$ 0.00051 | $\pm$ 0.00001 |
| $\delta m_d$ | 0.472 $ps^{-1}$ | $\pm$ 0.017 | $\mp$ 0.00003 | $\pm$ 0.00008 |
| $\chi$ | 0.1177 | $\pm$ 0.0055 | $\pm$ 0.00082 | $\pm$ 0.00001 |
| Lepton identification / $p_T$ / Background | | | **0.0009** | **0.0044** |
| Misidentified $e$ | | see text | $\pm$ 0.00011 | $\pm$ 0.00021 |
| Converted photons in $e$ sample | | $\pm$ 10 % | $\mp$ 0.00019 | $\mp$ 0.00050 |
| Misidentified $\mu$ | | see text | $\pm$ 0.00025 | $\pm$ 0.00085 |
| $\pi$,$K$ decay rate in Mu | | $\pm$ 15% | $\pm$ 0.00027 | $\pm$ 0.00092 |
| $p_T$ reweight of background | | see text | $\mp$ 0.00007 | $\pm$ 0.00021 |
| background asymmetry | | $\pm$ 40 % | $\mp$ 0.00076 | $\pm$ 0.00421 |
| Energy flow correction | | see text | $\mp$ 0.00009 | $\mp$ 0.00020 |
| Btag and jet charge calibration | | | **0.0011** | **0.0014** |
| Btag tunning | | see text | $\mp$ 0.00009 | $\pm$ 0.00028 |
| Merging for $N_{int} = 2$ | | see text | + 0.00061 | − 0.00082 |
| Jet charge stat | | see text | $\mp$ 0.00077 | $\pm$ 0.00102 |
| Jet charge BKG substraction | | see text | $\mp$ 0.00041 | $\pm$ 0.00040 |
| total | | | **0.0023** | **0.0058** |

Table 7: Different systematics in the $\chi^2$ fit of the 1993-1995 DELPHI lepton sample at $\sqrt{\rm s} = 91.22$ GeV . The systematics at $\sqrt{\rm s} = 89.43$ GeV were estimated to be $\pm$ 0.0024 for $A_{\rm FB}^{\rm b\bar{b}}$ and $\pm$ 0.0046 for $A_{\rm FB}^{\rm c\bar{c}}$ , and at $\sqrt{\rm s} = 92.99$ GeV $\pm$ 0.0024 and $\pm$ 0.0070.

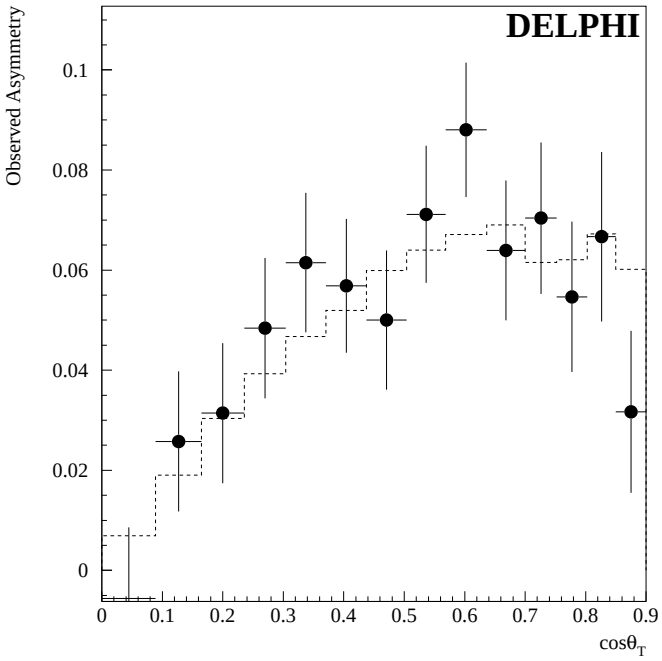


Figure 5: *Observed $A_{FB}^{obs}$ asymmetry at peak energy in various bin of* $\cos\theta_T$ *for a data subsample enriched in b with the right sign ($\mathcal{P}_{b_r} - \mathcal{P}_{b_w} > 0.6$). The result of the fit is quoted as a dashed line.*

# 7 Systematics effects

The systematics from the different sources are listed in table 7.

**Lepton sample**

To estimate the systematics due to uncertainties in decay branching ratios and spectra, the standard prescription of the LEP Heavy Flavour Working group was used [13]. The central values and variation were taken from [14] and [12], including for the $b$ and $c$ decay model. The variation considered for the lepton identification was described in section 3.

**Mixing**

The combined effect of the uncertainties quoted in table 7 for the parameters having a direct effect on the $B-\bar{B}$ mixing description end up to precision of 1.4% on $f_{B_s^0}$ and 0.005 on $\chi$ [12]. To take into account correctly the impact of the different sources of uncertainty on the mixing description, each of these measurements was varied within its error.

**Background Asymmetry**

It should be noted that, while the observed "Background Asymmetry" systematic in $A_{\rm FB}^{\rm c\bar{c}}$ comes from background in *uds* events, for $A_{\rm FB}^{\rm b\bar{b}}$ the main responsible is the charge correlation between the fake leptons and the initial quark in $b$ events themself.

Even if the charge correlation between the fake leptons and the initial quark of the corresponding event has been taken from the simulation, such correlation can be studied in data using the $Q_\ell \times Q_{opp}$ observable. From these studies a change of 20% in the correlation (= 40% in the background asymmetry) has been considered for the systematics. For example such change increases by 1.8 the $\chi^2$ of the data/simulation comparison computed from the figure 3 corresponding to $b$ events enriched in fake lepton by $p/p_T$ cuts. The

same comparison done in the $b$-tag bin I, enriched in fake leptons from $uds$ events, gives an increase of 1.3 of the $\chi^2$.

**Energy flow, $p_T$ reconstruction**

Due to a slightly worse energy reconstruction in the data, a 1-2 % shift in the jet energy distribution between data and simulation has been observed. This difference could have different effects on the asymmetries depending on its exact source ( overall correction or sub-sample of charged/neutral track correction ). The different possible sources were considered and the biggest effect observed was taken as systematics.
In the anti-b-tagged sample the shape of the $p_T$ distribution of the lepton candidate was not correctly described by the simulation. This effect is known to be common to all tracks from hadronisation in the tuned DELPHI simulation [7]. The full size of the correction estimated in the anti-b-tagged sample, was considered as systematics. It corresponds to changes $\sim \pm 5\%$ of the number of miss-identified lepton in function of the $p_T$.

**b-tagging**

To take into account the effect of changes in the fraction $r_q$, defined in equation 5, the b-tagging corrections, $\delta_q^{(i)}$, were recomputed for each of the changes quoted in table 7. For this reason all the quoted systematics include also possible variations induced by changes in the b-tagging tuning.

The systematics named *Btag tuning* in table 7, corresponds to the effects of the finite simulation statistics used to estimate the sample composition in the different b-tagged intervals and to the sensitivity to the correlation $\rho_q^{(i)}$ as described in section 4.

The full difference between the results obtained for the two considered $N_{int} = 2$ systems (see section 4) is quoted as *Merging for* $N_{int} = 2$.

**Jet Charge**

Like for the b-tagging, to take into account possible effect on the jet charge tuning of the parameters variation quoted in table 7, the jet charge tuning was performed for each systematic computation.

The systematics named *Jet charge stat* in table 7, correspond to the effect of the finite statistics used to estimate $\sigma$ , $f$ and $m$. The systematics named *Jet charge BKG substraction* in table 7, correspond to the effect of a change in the $\sigma$ and $m$ of the background, when tuning the $b$ jet charge. The variation considered for these parameters is the one which could produce the differences observed in the anti b-tag interval between data and simulation for $Q_\ell \times Q_{opp}$.

# 8 Corrections to the measured asymmetries

The QCD corrections applied to the asymmetries were obtained following the prescription given in [15]. This approch takes into account changes in the QCD corrections due to experimental bias, like the suppression of events with energetic gluon induced by the cut on the momentum of the selected leptons. The simulation sample, with an enlarged asymmetry [8] to improve the statistical precision of the study, was used to estimate the bias to the QCD corrections. The scaling of the QCD corrections was estimated for this analysis to be $0.58 \pm 0.08$ for $A_{\rm FB}^{\rm b\overline{b}}$ and $0.42 \pm 0.12$ for $A_{\rm FB}^{\rm c\overline{c}}$ . These scale factors were

[8] A value of 0.73 was used, slightly smaller than the maximal asymmetry allowed (0.75) to avoid boundary problem and asymmetric errors in the result of the fit

applied to the theoretical QCD correction [9] and give the following QCD corrections : $A_{\rm FB}^{noQCD,x\overline{x}} = A_{\rm FB}^{x\overline{x}}/(1-C_x)$ with $C_b = 0.0205 \pm 0.0046$ and $C_c = 0.0172 \pm 0.0057$ .

# 9 Conclusion

The heavy flavour asymmetry measurements presented in this paper, obtained with the 1993-1995 DELPHI data, can be combined with the 1991-1992 DELPHI measurements of $A_{\rm FB}^{b\overline{b}}$ and $A_{\rm FB}^{c\overline{c}}$ using leptons [2]. All asymmetries before average were QCD corrected and the 1991-1992 DELPHI measurements were corrected to the same inputs (branching ratios and mixing) than the one used in this paper.

Taking into account the correlations between the different systematics sources, the combined results are:

$$\begin{array}{lcllllllll}
A_{\rm FB}^{b\overline{b}} & = & 0.067 & \pm & 0.022 & (\text{stat}) & \pm & 0.002 & (\text{syst}) & \text{at } \sqrt{s} = 89.43 \text{ GeV} \\
A_{\rm FB}^{b\overline{b}} & = & 0.1004 & \pm & 0.0056 & (\text{stat}) & \pm & 0.0025 & (\text{syst}) & \text{at } \sqrt{s} = 91.26 \text{ GeV} \\
A_{\rm FB}^{b\overline{b}} & = & 0.112 & \pm & 0.018 & (\text{stat}) & \pm & 0.002 & (\text{syst}) & \text{at } \sqrt{s} = 92.99 \text{ GeV} \\
A_{\rm FB}^{c\overline{c}} & = & 0.031 & \pm & 0.035 & (\text{stat}) & \pm & 0.005 & (\text{syst}) & \text{at } \sqrt{s} = 89.43 \text{ GeV} \\
A_{\rm FB}^{c\overline{c}} & = & 0.0631 & \pm & 0.0093 & (\text{stat}) & \pm & 0.0065 & (\text{syst}) & \text{at } \sqrt{s} = 91.26 \text{ GeV} \\
A_{\rm FB}^{c\overline{c}} & = & 0.110 & \pm & 0.028 & (\text{stat}) & \pm & 0.007 & (\text{syst}) & \text{at } \sqrt{s} = 92.99 \text{ GeV}
\end{array}$$

Following the general procedure described in [13], the previous results have been corrected to the $Z$ pole and the effects of initial state radiation, $\gamma$ and $\gamma/\ Z$ exchange have been substracted. The averages of the pole asymmetries obtained after these corrections are :

$$\begin{array}{lcllllll}
A_{\rm FB}^{0,b} & = & 0.1021 & \pm & 0.0052 & (\text{stat}) & \pm & 0.0024 \quad (\text{syst}) \\
A_{\rm FB}^{0,c} & = & 0.0728 & \pm & 0.0086 & (\text{stat}) & \pm & 0.0063 \quad (\text{syst})
\end{array}$$

The total correlation between $A_{\rm FB}^{0,b}$ and $A_{\rm FB}^{0,c}$ is +7% , with a correlation of respectively +22% and -36% for the statistical and systematical errors.

The effective value of the Weinberg mixing angle derived from these measurements was

$$\sin^2\theta_{\rm W,eff}^{lept} = 0.23169 \pm 0.00010$$

[9] $C_b^{had,T} = 0.0354 \pm 0.0063$ and $C_c^{had,T} = 0.0413 \pm 0.0063$ as recommanded in [14].

# References


[1] DELPHI Collaboration, P.Abreu *et al.*, Phys. Lett **B276** (1992) 536.

[2] DELPHI Collaboration, P.Abreu *et al.*, Z. Phys **C65** (1995) 569.

[3] DELPHI Collaboration, P. Abreu *et al.*, Nucl. Inst. Meth. **A303** (1991) 233;
DELPHI Collaboration, P. Abreu *et al.*, Nucl. Inst. Meth. **A378** (1996) 57.

[4] N. Bingefors *et al.*, Nucl. Inst. Meth. **A328** (1993) 447.

[5] V. Chabaud *et al.*, Nucl. Inst. Meth. **A368** (1996) 314.

[6] T. Sjöstrand, Comp. Phys. Comm. **82** (1994) 74.

[7] DELPHI Collaboration P. Abreu *et al.*, Zeit. Phys. **C73** (1996) 11.

[8] Jade Collaboration, W. Bartel et al., Z. Phys. **C33** (1986) 23;
Jade Collaboration, S. Bethle et al., Phys. Lett. **B213** (1988) 235.

[9] DELPHI Collaboration, P.Abreu *et al.*, E. Phys. J. **C10** (1999) 415.

[10] DELPHI Collaboration, P.Abreu *et al.*, E. Phys. J. **C9** (1999) 367.

[11] The ALEPH, CDF, DELPHI, L3, OPAL and SLD Collaborations (D. Abbaneo *et al.*), *Combined results on b-hadron production rates and decay properties*, CERN EP2001-050.

[12] The Particle Data Group, D.E.Groom et al., E. Phys. J. **C15** (2000) 1.

[13] The LEP Experiments: ALEPH, DELPHI, L3 and OPAL, Nucl. Inst. Meth. **A378** (1996) 101.

[14] The LEP/SLD Heavy Flavour Group, D. Abbaneo *et al.*, *Final Input Parameters for the LEP/SLD Electroweak Heavy Flavour analyses* , LEPHF/2001-01, http://www.cern.ch/LEPEWWG/heavy/lephf0101.ps.gz.

[15] LEP Heavy Flavour Group, D. Abbaneo *et al.*, Eur. Phys. J. **C4** (1998) 2, 185.